Journal of Membrane Science & Research

journal homepage: www.msrjournal.com

Research Paper

Preparation and Characterization of CA−PEG−TiO_2 Membranes: Effect of PEG and TiO_2 on Morphology, Flux and Fouling Performance

Kibrom Alebel Gebru, Chandan Das*

Department of Chemical Engineering, Indian Institute of Technology Guwahati-781039, Assam, India

ARTICLE INFO

Received 2016-09-09
Revised 2016-10-31
Accepted 2016-11-24
Available online 2016-11-24

KEYWORDS

CA membrane
Thermal stability
TiO_2 NPs
Polyethylene glycol
Anti-fouling

GRAPHICAL ABSTRACT

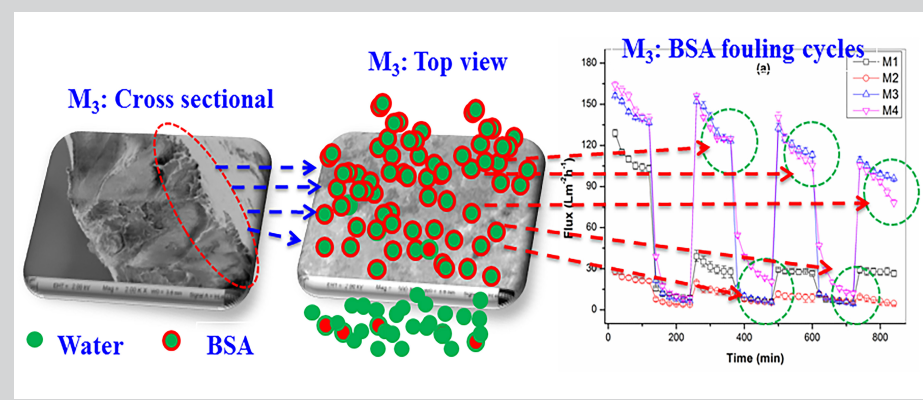

HIGHLIGHTS

- CA-PEG-TiO_2 membrane exhibited highest thermal degradation temperature
- Improved PWF, porosity, hydrophilicity attained after PEG and TiO_2 were added.
- CA-PEG-TiO_2 exhibited highest BSA flux and recoveries for three fouling cycles.

ABSTRACT

Modified cellulose acetate (CA) membranes were prepared by dissolving the polymers in a mixture of acetone (AC) and N, N dimethylacetamide (DMAc) (70:30) solvent and deionized (DI) water was used in the coagulation bath. The introduction of polyethylene glycol (PEG) additive and TiO_2 nanoparticles (NPs) into the casting solution has changed the structures of the resulting membranes during the phase inversion process. Effects of PEG additive and TiO_2 NPs on the preparation of the phase-inverted CA ultrafiltration membrane were investigated in terms of morphology, equilibrium water content (EWC), pure water flux (PWF), hydraulic resistance, thermal stability, water contact angle (WCA) and anti-fouling performance. Improvements in average pore size, porosity, thermal stability, and the hydrophilic nature of the CA membranes was detected after the introduction of PEG and TiO_2 simultaneously to the polymer matrix. Thermo gravimetric analysis (TGA) results confirmed that the interaction between TiO_2 and the degradation temperature of the CA membrane were significantly improved. The anti-fouling performance and the flux recovery potential of the membranes were investigated using the bovine serum albumin (BSA) protein. The M3 (CA-PEG-TiO_2) membrane (10.5 Wt. % CA: 4 Wt. % PEG: 2 Wt. % TiO_2) exhibited the highest BSA flux result and normalized flux recovery ratios (NFR) for the three fouling cycles.

1. Introduction

Synthetic membranes in general and ultrafiltration (UF) membranes have specifically received more attention in various applications, such as wastewater treatments, bio-separation, recovery of proteins, clarification of fruit juice and alcoholic beverages, separation of oil-water emulsions, food and paper industry [1]. The principle of fabrication of asymmetric polymeric membranes is based on the phenomenon of phase inversion [2]. The common techniques of the precipitation of polymer are immersion precipitation, thermally induced phase inversion, vapor induced phase inversion, and dry casting of polymer solution [3]. The most commonly available commercial membranes are prepared by phase inversion [4]. Cellulose acetate is broadly applicable for the synthesis of membranes because of having tough, biocompatible, hydrophilic characteristics, good desalting nature, high flux, and is moderately less expensive to be employed for reverse osmosis, microfiltration, ultrafiltration and gas separation applications [5]. The drawback of cellulose acetate membranes is that they are susceptible to thermal and mechanical stabilities depending on the environments and conditions of application [6]. Generally, the presence of the polymeric additive increases the concentration/viscosity of the casting solution which may diminish the diffusional exchange rate of the solvent and non-solvent

* Corresponding author at: Phone: +91 361 2582268; fax: +91 361 2582291
E-mail address: cdas@iitg.ac.in (C. Das)

DOI: 10.22079/jmsr.2016.22820

during the membrane formation process [7]. Liu et al. [8] have studied the morphology controlled characterization of the polyethersulfone hollow fiber membrane by the introduction of polyethylene glycol. In their study, they have shown that PEG can be used as an additive to improve the polymer (PES) dope viscosity and to develop the pore inter-connectivity. Panda and De carried out a detailed investigation on the effect of polyethylene glycol in polysulfone membranes. The influences of PEG molecular weight, solution concentration, the type of solvents, and thickness of casting solution were explored. As the solubility of the solvent and non-solvent can play significant roles in the morphology of the resulting membrane, higher solubility of the solvent: non-solvent leads to a rapid de-mixing. On the other hand, a delayed de-mixing may occur due to poor solubility and result in a membrane with a denser top layer. Due to the higher solubility between NMP and water than that of the DMF and water, the exchange ratio between NMP/PES is higher than the DMF/PES ratio, which implicates more diffusion between the solvent and polymer and the formation of a porous membrane. Thus, a highly porous membrane was achieved using N-methyl-2-pyrrolidone (NMP) as a solvent when compared to N, N-dimethylformamide (DMF) [9]. Chakrabarty et al. [10], on the other hand, have prepared flat sheet asymmetric polymeric membranes from a homogeneous solution of polysulfone by the phase inversion method. Their results have shown that the membranes with higher molecular weights of PEG resulted in high pure water flux because of the higher porosity of the membranes. Saljoughi et al. [7] have prepared asymmetric CA membrane from blends of CA, PEG, and NMP using the immersion precipitation phase-inversion process. From their observations, an increase in PEG concentration in the casting solution alongside a higher coagulation bath temperature resulted in improvement of the pure water flux, membrane thickness, and human serum albumin transmission. Using organic-inorganic membranes, the separation properties of polymeric membranes can be enhanced and may possess properties such as selectivity, good permeability, thermal and chemical stability and mechanical strength [11]. Another challenge in the field of membrane process is fouling. Since membrane fouling causes a severe decline of the solvent flux, it becomes essential to fabricate membranes less susceptible to fouling by making some modification during preparation. In ultrafiltration processes, several attempts have been accomplished to decrease fouling, which in general include feed solution pre-treatment, membrane surface enhancements and process modifications [12]. In recent researches, it is confirmed that the introduction of nanoparticles in a membrane matrix develops the membrane hydrophilicity, anti-fouling property, and permeability. Accordingly, several inorganic oxide nanoparticles such as Al_2O_3 [13] , ZrO_2 [14], TiO_2 [12], and SiO_2 [15] have been added within the polymer casting solution. Prince et al. have prepared the functionally modified PES hollow fiber membrane using PEG 400 and silver (Ag) NPs through thermal grafting. The attachment of PEG additive and silver NPs on the surface of the PES hollow fiber membranes were done by using poly (acrylonitrile-co-maleic acid) (PANCMA) as a chemical linker. The WCA results of the modified membranes were found to be decreased by about 75.5 % from 62.6±3.7 º to 15.3±1.2 º and the PWF have improved by around 36% from 513 L/m^2h to 702 L/m^2h [16]. On the other hand, Garcia-Ivars et al. have prepared UV irradiation modified polyethersulfone (PES) UF membranes using two nano-sized hydrophilic compounds viz. PEG and Al_2O_3 NPs. The WCA and pore size results of the modified membranes have decreased indicating an enhancement of the hydrophilicity nature of the resulting membranes. Furthermore, the PEG solute flux and rejection of the PES membranes were enhanced due to UV photo grafting. Moreover, the modified PES membranes (i.e. 2.0 wt. % PEG and 0.5 wt. % Al_2O_3) have exhibited superior anti-fouling performance than the other tested membranes [17]. Current researchers have paid attention to TiO_2 due to its stable nature, being easily available and the potential for different applications. Moreover, TiO_2 can enhance the hydrophilicity of different polymers to improve flux and decrease the fouling problem which are important parameters in water and wastewater treatment [12]. In the membrane filtration process, factors like thermal/chemical, fouling and flux are very important properties and the current study is focused on improving these properties simultaneously.

From the above literature, it is observed that there is no report on the preparation and characterization of phase inverted CA-PEG-TiO_2 composite membranes. Although some studies on the preparation of polymer/NPs membranes have been previously done, the preparation of membranes from CA, PEG as additive and TiO_2 NPs need to be investigated (i.e. to enhance the morphological structure and anti-fouling performance). As far as the authors' knowledge is concerned, this work is the first report on the preparation of the composite ultrafiltration membrane from CA, PEG, and TiO_2 with a detailed explanation. Therefore, effort was made to investigate the influence of PEG and TiO_2 on the morphological structure, permeability performance, and thermal stability property of the membrane in addition to the anti-fouling properties of CA-PEG-TiO_2 membranes.

2. Experimental

2.1. Materials

Cellulose acetate polymer was purchased from Loba Chemie, India. The two solvents, namely, N, N-Dimethyl acetamide (DMAc) and acetone (AC) (both with an analytical purity of 99 %); polyethylene glycol 4000 were all obtained from Merck Specialties Private Limited, Mumbai, India; TiO_2 with a purity of 99.5 % were obtained from Sigma-Aldrich Co., USA. Deionized water (DI) was used as the non-solvent in the coagulation bath throughout this experiment, which was purified using the Millipore system. Bovine serum albumin (BSA) protein having a molecular weight of 66 kDa was purchased from SRL, India.

2.2. Membrane preparation

The phase inversion technique by immersion precipitation was used for fabrication of the asymmetric UF membrane from cellulose acetate polymer. Initially, uniform solutions of CA in Acetone/DMAc (70/30; v/v) were prepared under continuous magnetic stirring at room temperature (25 ±2 ºC). The casting solution was stirred overnight using a magnetic stirrer at room temperature. After that, the solutions containing CA, solvents and additives (PEG and TiO_2 NPs) became homogeneous, and they were kept at room temperature for one day to avoid air bubbles. Subsequently, the casting solution was poured consistently on a glass sheet and carefully cast using a casting knife keeping a gap of roughly about 0.25 mm between the knife and glass plate. The resultant films were exposed to air for approximately 30 s earlier to immersing to the coagulation bath comprised of DI water at room temperature. In the coagulation bath, the cast solution turned from transparent to white color for membranes CA and CA-PEG. On the other hand, the milky color for CA-TiO_2 and CA-PEG-TiO_2 membranes was changed to white, and all the thin films were detached from the glass plate. The membrane sheets were kept in the coagulation bath for 30 min. After that, the prepared membranes were put in DI water filled beakers until use. Finally, the membrane films were cut into circular discs to be placed in the membrane cell for UF experiments. The membranes with different composition are designated as, M_1, M_2, M_3 and M_4 (i.e. CA, CA-TiO_2, CA-PEG-TiO_2, and CA-PEG, respectively). Table 1 shows the solution casting compositions of CA, PEG and TiO_2 nanoparticles. The flow diagram for the membrane preparation process is presented in Figure 1. The amounts of CA, PEG and TiO_2 NPs were selected based on the previous works [7, 18].

Table 1
Solution compositions and viscosity of the casting solution: CA, PEG and TiO_2 nanoparticles.

Membrane	CA (wt.%)	TiO_2 (wt.%)	PEG (wt.%)	AC:DMAc (70:30; v/v)	Viscosity (mPa.s)
M_1	10.5	-	-	89.5	1680
M_2	10.5	2	-	87.5	3180
M_3	10.5	2	4	83.5	1850
M_4	10.5	-	4	85.5	1781

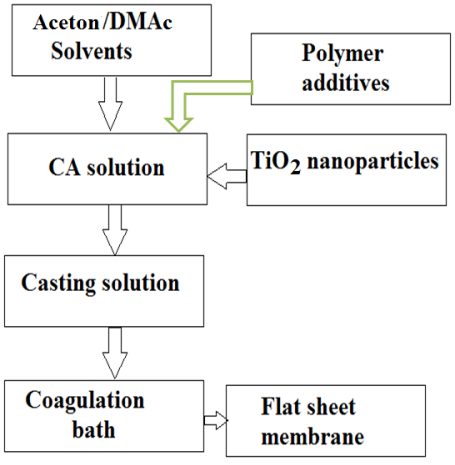

Fig. 1. Flow diagram of the preparation method of flat sheet membranes.

2.3. Characterization of membranes

2.3.1. Hydrophilicity and porosity measurements

To study the hydrophilic nature and porosity of the prepared membranes, three parameters were applied namely, water contact angle (º), equilibrium water content (EWC), and membrane porosity (ε). Both the ε and hydrophilicity play significant roles in the permeability and rejection nature of the membrane. The water contact angle (WCA) measurements of the prepared membranes were conducted on a contact angle measuring instrument (Kruss, advance drop shape analysis, Germany). The stability of the TiO_2 NPs incorporated within the matrix of the modified membranes was studied qualitatively. All the prepared membranes were soaked in DI water for 8 days at room temperature (25 ± 2 ºC). The WCA values of all the membranes were done and the TiO_2 leaching tendency during each soaking period was evaluated [17]. On the other hand, the EWC and ε were evaluated using a simple gravimetric method, where each membrane sample (2.5×2.5 square cm) was immersed in DI water beakers for a specified period. Then, the samples were dabbed with dry filter paper and weighed immediately (W_w). Finally, the membranes were kept inside vacuum atmosphere for 24 h at 50 ºC. The final dry weights of the samples (W_D) have been taken again. The membrane porosities were calculated by dividing the volume of the pores by the total volume of the membrane. Therefore, the results are found using the following equation [19]:

$$\varepsilon(\%) = \frac{[(W_W - W_D)/\rho_W]}{[(W_W - W_D)/\rho_W] + [W_D/\rho_P]} \times 100 \quad (1)$$

where, W_W is the wet membrane weight (g), W_D is the dry membrane weight (g), ρ_W is the pure water density at working condition (g cm^{-3}), and ρ_p is the polymer density (g cm^{-3}). As discussed earlier, EWC was calculated using the subsequent equation [10]:

$$EWC(\%) = [(W_W - W_D)/W_W] \times 100 \quad (2)$$

The average values of EWC and membrane porosity were taken after measuring five different samples of each membrane to reduce the error of the balancing measurement.

2.3.2. Average pore radius determination

The water filtration velocity method was employed to determine the average pore size of the membranes and the results were calculated at constant transmembrane pressure (300 kPa). Generally, the membrane average pore radius (r_m) is considered as an approximation of true pore size and it denotes the average pore size throughout the membrane thickness (ζ). The average pore radius can be calculated by using the Guerout–Elford–Ferry equation [20]:

$$r_m = \sqrt{\frac{[(2.9 - 1.75\times\varepsilon)(8\times\mu\times\zeta\times Q_W)]}{(\varepsilon\times A_m\times\Delta P)}} \quad (3)$$

where μ is the water viscosity (8.9×10^{-4}) in Pa. s, Q_W is the pure water flow ($m^3\ s^{-1}$) and ΔP is the transmembrane pressure (300 kPa).

2.3.3. Pure water flux study

In this study, a batch cell experimental set-up was used, which is presented schematically in Figure 2. This experimental set-up is comprised of a pressure source to supply the pressure required for the filtration experiment; the feed tank where the feed is collected; filtration cell, membrane piece and permeate after membrane filtration. A pure water permeability experiment was done in a 400 mL stirred batch cell. Membranes with a circular shape of 7×10^{-2} m diameter and with effective filtration area of 3.85×10^{-3} m^2 were employed for this experiment. Compaction studies of each prepared membrane were done using deionized water for 2 h using a fixed pressure of 300 kPa and pure water flux results were recorded with a 10 min interval. The membrane compaction factors (CF) were found by calculating the ratio of initial pure water flux (J_{wi}) to steady state pure water flux (J_{wf}). Pure water flux results were calculated using the following equation:

$$J_W = [Q/(A\times\Delta t)] \quad (4)$$

where, J_w is pure water flux (L/m^2 h), Q is the volume of water permeated (L), A is the effective membrane area (m^2) and Δt is permeation time (h). Thus, pure water fluxes were evaluated by means of passing deionized (DI) water through the membranes. Pure water flux values at different transmembrane pressures (ΔP) (ranging from 100 to 300kPa) were recorded. Membrane resistance (R_m) results were calculated according to Darcy's law (Eq. (5)):

$$R_m = [\Delta P/(\mu\times J_W)] \quad (5)$$

where μ is the water viscosity (8.9×10^{-4}) in Pa s.

2.3.4. Morphological studies

Morphological studies of the prepared membranes were done using a high-resolution field emission scanning electron microscopy (FESEM, ZEISS, USA), which provides visual information of the topographic structure besides the cross-sectional structure of the prepared membranes. The elemental composition analysis was done by using high-energy electrons of the energy dispersive X-ray spectroscopy (EDS, ZEISS, USA). For both the analyses, a gold coating for the samples was done by means of a high-resolution sputter coater, Quorum, to protect the membranes from charging during the image analysis. Finally, the pieces of membranes were attached to a plate holder using double-sided adhesive carbon tape in a horizontal position.

2.3.5. Thermogravimetric analysis

The thermal degradation analysis was conducted by thermo-microbalance (Thermo gravimetric Analyzer) (TG 209 F1 Libra®, Germany). The TGA results were found from 30 to 800 ºC using nitrogen gas where the flow rate was kept as 40 mL/min at a heating rate of 10 ºC/min. All the membranes were loaded into a platinum sample holding pan.

2.3.6. Fouling and rejection performances

Membrane fouling experiments were done in the stirred ultrafiltiration batch cell (Figure 2) to investigate the effect of PEG and TiO_2 on protein rejection and permeate flux of the prepared membranes. The concentration and the pH of BSA solutions were 1 g L^{-1} and 7.0, respectively, throughout the experiments and DI water was used as solvent for BSA. The flux values were calculated using Eq. (4) and the rejection of BSA solutions was evaluated by Eq. (6).

$$R(\%) = [(1-(C_p/C_f)]\times100 \quad (6)$$

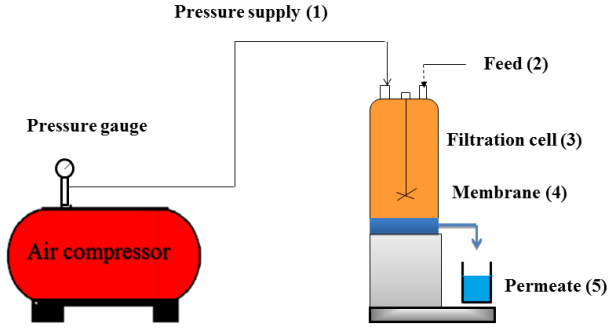

Fig. 2. Schematic diagram of the batch experimental set-up.

where, C_p and C_f are the concentrations (mg L^{-1}) in the permeate side and the feed side, respectively. Subsequently, the feed and permeate concentrations of BSA solution were evaluated by using the UV–vis spectrophotometer (Thermo Fisher Scientific, UV2300, India) at a wavelength of 278 nm. These experiments were repeated for three times and the error bars are presented. To investigate the anti-fouling properties of the prepared membranes, the flux losses due to total fouling (F_t, reversible fouling (F_r), and irreversible fouling (F_{ir}) of all the three cyles were calculated using the following equations, respectively [21].

$$F_t = [1-(J_B/J_{Wi})] \quad (7)$$

$$F_r = [(J_{Wf} - J_B)/J_{Wi}] \quad (8)$$

$$F_{ir} = [(J_{Wi} - J_{Wf})/J_{Wi}] \quad (9)$$

The fouling resistant capacity of the prepared membranes was evaluated using normalized flux ratio (NFR) as shown in Eq. (10).

$$NFR(\%) = [(J_{Wf} / J_{Wi}) \times 100] \quad (10)$$

where J_B is the BSA flux; J_{Wf} is the flux of the membrane after fouling (2 h); and J_{Wi} is the flux of the membrane found at the start of each fouling stage. Normally, a greater NFR value (next to 1) indicates a better anti-fouling nature of the membranes.

2.4. Characterization of TiO_2 NPs

The particle size of TiO_2 nanoparticles (commercial) was characterized by using transmission electron microscopy (TEM, JEOL, JEM 2100, USA) at 210 kV. First, the TiO_2 nanoparticle sample was prepared by dispersing in DI water (500 mg/L) and then being poured on a carbon tape covered plate. Finally, the sample was dried at room temperature and ready for TEM analysis. As clearly shown in Figure 3, the TiO_2 NPs appeared in the form of spots. To measure the size of each nanoparticle, ImageJ software was employed, their sizes ranging from 16 to 72 nm. The average particle size was approximately 29.8 nm.

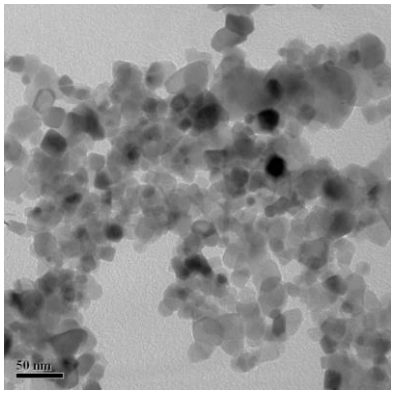

Fig. 3. TEM image of commercial TiO_2 nanoparticles.

3. Results and discussion

3.1. Morphological study

FESEM analysis is an important method to study the membrane morphological structure and qualitative information about surface and cross-sectional morphology of the membranes to be achieved. The top layer surface view, the cross-sectional view, and elemental analysis results of the prepared membranes by dissolving the polymer and additives in AC: DMAc are presented in the FESEM and EDS images (i.e., Figure 4(a), (b) and (c) respectively). As evidently revealed from the figures, the synthesized membranes are asymmetric in structure involving a dense top layer and a porous sub-layer for all types of membranes.

3.1.1. Effect of PEG and TiO_2 NPs

The sub-layer portion of the M_1 membrane appears to have finger-like voids as well as macro-void structures. Generally, the development of macro-voids happens under rapid precipitation conditions, and the precipitations are quicker at high coagulation temperature [7]. In the present study, the coagulation bath temperature and evaporation time (i.e. before immersion) were fixed to 25±2 ºC and 30 s, respectively, during the preparation of all the membranes. An additional significant factor which can affect the formation or suppression of macro-voids is the type of de-mixing occurred during the phase separation process, where, the instantaneous de-mixing and the delayed de-mixing depend on the mutual affinity of the solvent and non-solvent in the ternary system [4]. In the solvent and polymer interaction scheme, three kinds of interactions viz. polymer: polymer, polymer: solvent and solvent: non-solvent are applied. If good polymer solvents are used, the degree of polymer stretching reaches to its highest level and more favorable polymer/solvent interactions can occur. The solvents used in this study (i.e. AC: DMAc) have high mutual affinity with water [22]. Thus, apparently, the development of the finger-like voids and macro-voids in the sub-layer of the M_1 (additive free) membrane is due to the instantaneous de-mixing. In this case, the CA (additive free) stretches to its highest level where there is a maximum interaction between the CA and AC: DMAc, which tends to instantaneous de-mixing conditions to happen. On the other hand, after adding the PEG and TiO_2 to the ternary (polymer/solvent/non-solvent) system, the developments of macro-voids are suppressed significantly (i.e. M_2, M_3 and M_4). The presence of the polymeric additives and TiO_2 NPs can increase the concentration/viscosity of the casting solution, which may diminish the diffusional exchange rate of the solvent and non-solvent during the membrane formation process. Accordingly, this may hamper the instantaneous liquid-liquid de-mixing process which suppresses the development of macro-voids [23]. However, for membranes prepared using PEG and TiO_2 nanoparticles (M_3) and without TiO_2 nanoparticles (M_4), the formation of micro-voids (microporous structure, which is important for the porosity of a membrane) was observed. It is clear that the pore forming properties of the PEG polymer have played a key role in the development of the porous sublayer. A quaternary system (polymer/solvent/non-solvent/additive) of the phase separation involves de-mixing of the entangled polymers. In this quaternary system, two phases occur from the phase separation; one involves CA (i.e. membrane forming polymer), AC: DMAc (i.e. solvent) and non-solvent; the second contains the additive (i.e. PEG), AC: DMAc and non-solvent. The membrane forming polymer and additive has a dynamic strength to be completely separated to CA-rich and PEG-rich phases. Consequently, the type of de-mixing process can also be decided by the diffusion of these polymers with respect to each other. On the other hand, the addition of TiO_2 to the membrane formation system has its influence on the de-mixing process. However, almost macro-void free cross-sectional structures were observed for the M_4 system. From these results, it can be concluded that although the instantaneous de-mixing is still continued, the effect of the PEG has a substantial role in the suppression of the finger-like structure and macro-voids which occurred for the M_1 membrane. The presence of the polymeric additive increases the concentration/viscosity of the casting solution, which may diminish the diffusional exchange rate of the solvent and non-solvent during the membrane formation process. Consequently, this may hinder the instantaneous liquid-liquid de-mixing process which suppresses the development of macro-voids [7]. On the other hand, the comparatively low affinity of PEG to the solvents may take additional time to reach the top surface allowing the polymeric molecule to get sufficient time to accumulate and re-arrange and subsequently develop a relatively thicker and denser top layer. The open pore structures developed in the membranes are formed by nucleation and development of the polymer-lean phase in the metastable area between the bi-nodal and the spinodal curve [24, 25]. A possible explanation for the formation of a nodular structure on the top surface of the membranes could be due to the spinodal de-mixing because the diffusion process throughout the development of the top-layer is faster for the homogenous system to become highly unstable and crosses the spinodal curve [24]. In the present study, the top surface with some open pore structures is observed more prominently in the case of PEG (i.e. M_3 and M_4) which is attained because of the spinodal decomposition. Therefore, the inter-connected pores may be accounted as a constant CA-lean/ PEG-rich phase entwined by a continuous CA- rich/ PEG-lean phase which is responsible for developing the uniform matrix of the membrane [8]. On the other hand, in the case of M_1 and M_2 membranes, no open pore structure was detected, where a less porous top surface structure was observed instead. On the other hand, it is evident from these figures that the finger-like structures and macro-voids are suppressed after adding TiO_2 (M_2 and M_3) regardless of the effect of PEG for the M_3 membrane. However, the M_2 membrane seems to have less microporous cross-sectional structures. These results are also confirmed by the porosity study (Table 2) where the M_2 membrane shows relatively lowest porosity than the other membranes. The introduction of both PEG and TiO_2 played an important role in the improvement of the membrane hydrophilicity and porosity. The porosity, EWC and pore radius results of the prepared membranes are calculated using Eq. (1), (2 and (3). The membrane average pore radius (r_m) is considered as an approximation of true pore size and the results are 23.6 nm, 15.6 nm, 35 nm and 31.4 nm for M_1, M_2, M_3 and M_4, respectively. Moreover, the lowest pore radius for the M_2 membrane is attributed to aggregation of some of the TiO_2 on the surface of the membrane pores. This can also be seen from the top surface view of M_2 presented in Figure 4a. Adding TiO_2 NPs to the polymeric solution can increase its viscosity. Therefore, the particles leaching problem is less, and subsequently, the pore forming effect of NPs can be declined in the case where the high viscosity of a solution hampers the development of pores and causes the porosity of the membrane to decrease [19]. To minimize the influence of thickness shrinkage of the polymer-phase due to the accumulation of NPs, in the present study, TiO_2 NPs having low concentration (i.e. 2 wt. %) were selected [26]. It may be worthy to mention here that the addition of NPs in the polymeric membrane may decrease or increase its viscosity depending on various parameters, such as concentration of additive and ligand stabilizer [27]. Due to the introduction of a relatively lower concentration of TiO_2, the finger-like structures, and macro-voids present in M_1 were greatly suppressed and a relatively dense layer with small finger-like structures was observed for M_3 and M_4. The presence of small macro-voids with a little finger-like structure in the case of M_3 and M_4 are assumed to be related to the

interference effect of NPs and PEG additive during the phase inversion process. Therefore, due to the interfacial stress between polymers and NPs, interfacial pores are formed as a result of shrinkage of polymer-phase during the de-mixing process [28]. However, the presence of TiO_2 in M_2 diminishes the presence of finger-like structures and a sublayer structure with almost free macro-voids is obtained. These results can be described in terms of the NPs agglomeration on the membrane forming the polymer matrix during the phase inversion process. The occurrence of the NPs agglomeration can be mainly caused due to the high surface energy of the NPs, which tend to aggregate for weakening their surface energy to reach a more stable state. Furthermore, the NPs agglomeration leads to a non-uniform dispersion of the NPs within the polymer surface and structure. This phenomenon can negatively change the resulting membrane properties such as hydrophilicity and surface roughness [26]. However, in the case of M_3 the NPs agglomeration was significantly minimized due to the improved distribution of the NPs because of the introduction of PEG additive [29].

3.2. Thermal stability studies

The thermal degradation analyses (i.e. TGA and DTG results) of all the prepared membranes are presented in Figure 5 (a) and (b), respectively. The graphs were plotted as weight loss (%) vs. temperatures (ºC). It can be clearly seen from the TGA figure that the decomposition of M_1 is shown in three steps. The first degradation step of the M_1 membrane was detected between 30 and 60 °C and the weight loss was about 4.5 %. This degradation is due to the presence of some volatile material or because of the evaporation of absorbed moisture by the sample. During the second degradation step, a high weight loss of around 16.5% was observed between 60 to 260 °C, which is possibly due to the start of the main thermal breakdown of CA chains. A final degradation step that started at 260 °C and ended at 380 °C with a weight loss of 79% was due to the main degradation and possibly because of the carbonization of the decomposition of the residual materials to ash. The TGA results of the M_1 membrane clearly show that it could be highly unstable at a high temperature and similar results were reported by Zafar et al. and Chatterjee et al. [30]. The TGA results of the CA membrane with PEG additive and TiO_2 displayed two-step degradation procedures. Therefore, the start of the decomposition step for M_2, M_3 and M_4 were 278 °C, 271 °C and 234 °C, respectively. The observed weight losses are due to the degradation of CA chains because of the pyrolysis of the back-bone of the CA polymer and also followed by de-acetylation of CA [31].

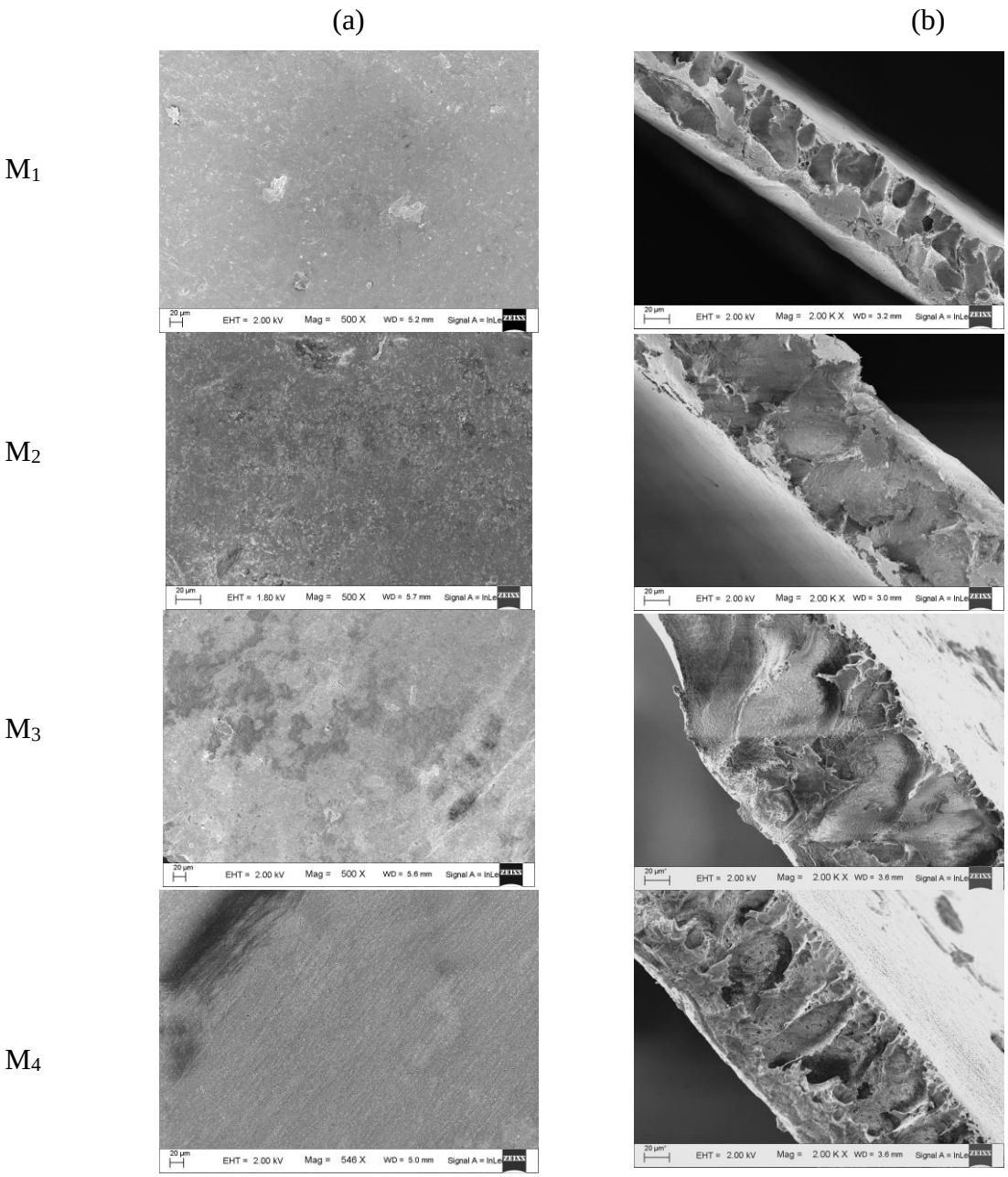

Fig. 4. (a) Top surface and (b) cross-sectional FESEM images (c) EDS results of M_1 (CA), M_2 (CA-TiO_2), M_3 (CA-PEG-TiO_2) and M_4 (CA-PEG) membranes.

(c)

M_1

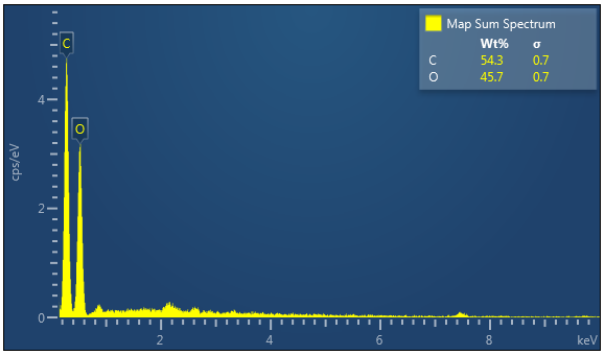

M_2

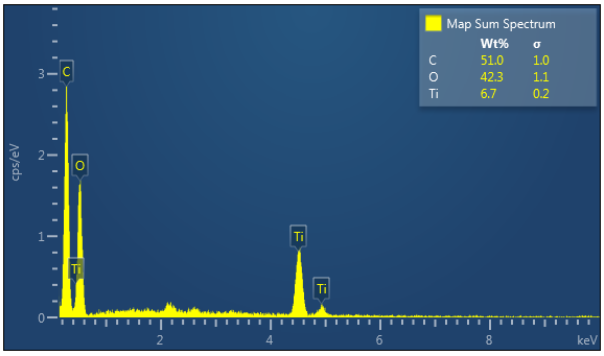

M_3

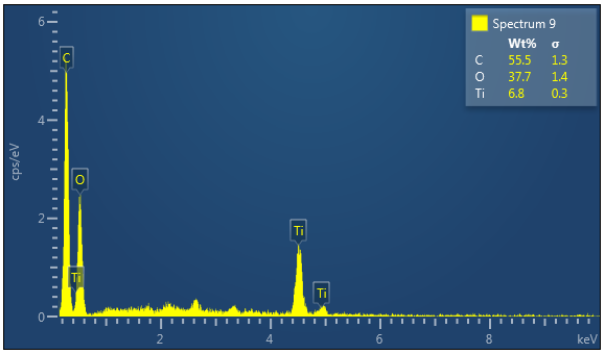

M_4

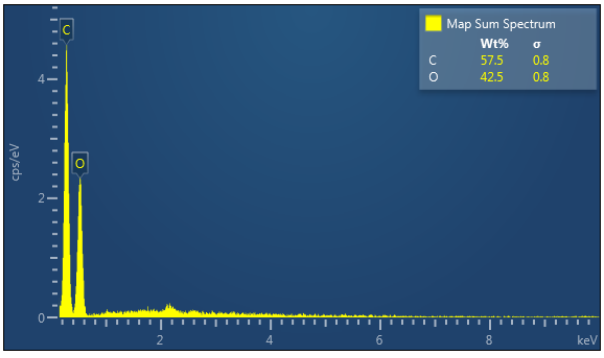

Fig. 4. Continued.

Table 2
Compaction and hydraulic characteristics of those prepared membranes at 250 kPa.

Membrane	CF	R_m ($\times 10^{-10} m^{-1}$)	J_w (L/m^2h)	EWC (%)	ε (%)	r_m (nm)	Thickness (μm)
M_1	1.50±0.4	0.90	204.5	77.8±1.5	81.9±2.0	23.6±5	83.5±8.0
M_2	4.50±0.2	4.30	21.1	76.7±2.6	81.0±2.5	15.6±7	102.4±4.2
M_3	1.66±0.3	0.70	530.7	79.5±1.2	83.4±1.8	35.0±3	84.2±6.5
M_4	1.52±0.4	0.67	265.3	79.0±1.4	82.9±1.9	31.4±4	126.9±3.0

During the last decomposition step, the degradation temperatures of M_2, M_3 and M_4 are 388 °C, 386 °C and 382 °C signifying the main thermal degradation of the CA chains, whereas the TiO_2 were totally stable until the end of the analysis (i.e. up to 800 °C). From these results, it is clearly noticed that the thermal degradation of the M_1 membrane was significantly enhanced due to the addition of PEG and TiO_2. An interesting observation from this study is that an increase in thermal stability after the addition of PEG to the CA membrane (M_4) is due to the presence of a trace amount of the PEG in the membrane matrix. The improved thermal stability of the M_4 membranes was due to the strong interaction between the CA and PEG in the membrane matrix by creating hydrogen bonds [32]. Moreover, the residuals, i.e. 0.08 %, 21.9 %, 19.6 % and 7.3 % for M_1, M_2, M_3 and M_4 are consistent with the thermal stability performances of the prepared membranes. Furthermore, the thermal stability of the M_3 membrane exhibited higher degradation temperature than the M_4 membrane. This result is attained due to the highly stable nature of TiO_2 at high temperatures and therefore the degradation temperature of the M_4 membrane was significantly improved after the addition of TiO_2. On the other hand, the slight improvement in degradation temperature for the M_2 membrane when compared with the M_3 membrane is that the less porous sublayer structure of the membrane is responsible for having strong resistance to heat flow than that of the porous membrane (M_3). In this study, the TGA and DTG plots clearly revealed that the thermal properties of the CA membrane were significantly improved after incorporation of PEG and TiO_2 into the CA solution.

3.3. Pure water flux performance

The membranes prepared by CA, CA-TiO_2, CA-PEG-TiO_2 and CA-PEG (M_1, M_2, M_3 and M_4, respectively), using AC: DMAc as solvent were investigated to evaluate the influence of PEG additive and TiO_2 NPs on PWF properties of the membranes. The membranes were characterized in terms of compaction factor, PWF and hydraulic resistance.

3.3.1. Effect of PEG and TiO_2 NPs

Studying the compaction factor (CF) of the prepared membranes is very essential to recognize the morphological structures (i.e. pore arrangements) of the membranes specially the membrane sub-layer configuration. Generally, membranes having high CF indicate that these are highly compacted and show the existence of some defective pores in the membrane sub-layer structure. The compaction factor and hydraulic characteristics of all the prepared membranes are presented in Table 2. It was observed that the CF of M_2 was greater (i.e. 4.5±0.2) which can also be explained due to the aggregation of NPs on the pore walls of the membrane could further block the pores after compaction. On the other hand, the CFs for the remaining membranes are almost similar except for the M_1 (1.5±0.4) which is slightly lower than M_3 (1.66±0.3) and M_4 (1.52±0.4). This result is achieved due to the existence of a more porous structure in case of M_3 and M_4 due to the introduction of PEG additive, where some of the pores were compacted after the compaction process. The introduction of additives into the membrane casting solutions may either suppress or increase the formation of macro-voids in the membrane sub-layer based on the type of additive [33]. The effects of PEG additive and TiO_2 NPs on PWF at different operating pressures are presented in Figure 6 (b). The results of PWF for all the membranes were increased almost uniformly with an increase in the operating pressure from 100 to 300 kPa. It is also shown that the PWF for membranes without PEG additive (M_1 and M_2) membranes are less than that of membranes with PEG additive (M_3 and M_4). Nevertheless, as the effect of the PEG additive, the CA-PEG-TiO_2 membrane shows higher pure water flux than that of the CA-TiO_2 membrane. These results are in a good agreement with the conclusions of the compaction study in Figure 6 (a). The hydraulic resistance (R_m), EWC, average pore radius, porosity and thickness of all the prepared membranes are reported in Table 2. As seen from these results, the hydraulic resistance of M_2 was greater than all the other membranes. This higher resistance of M_2 is because of its less porous nature than the other membranes that can resist the water flux as compared to the other membranes. Additionally, this result is supported by the average pore radius calculation (Eq. 3), where the result was 15.6 nm that is again less as compared with the other membranes. In addition, the R_m (m^{-1}) for the membranes without PEG additive (M_1) was higher than that of the membranes with PEG additive. Thus, the increase in hydraulic resistance and decrease in flux results of the membranes without PEG additive are obviously due to the decrease in average pore size and porosity as already explained in the previous sections. Generally, the PEG additive is more hydrophilic than the CA polymer. Therefore, the membranes with PEG additive displayed improved flux results. As shown in Table 2, by comparing the two membranes with PEG additive (M_3 and M_4), the CA-PEG-TiO_2 membrane gained slightly higher resistance and higher flux than the CA-PEG membrane. These results can be explained because the CA-PEG-TiO_2 membrane has a higher and more uniform porous and hydrophilic surface due to the introduction of TiO_2 NPs. On the other hand, as PEG additives were added and the whole additive would not be washed away during the membrane development due to its low solubility and diffusivity, it could exist inside the pores and within the membrane matrices. Therefore, the introduction of both PEG additive and TiO_2 NPs at the same time could play an important role in the improvement of the membrane hydrophilicity and porosity simultaneously. The porosity and EWC results of the prepared membranes results are calculated using Eqs. (1) and (2) and presented in Table 2. From the porosity measurement results, it is shown that all the membranes have shown satisfactory results in the range of 81 to 83.4 %, which is accredited to the lower concentration of the membrane forming polymer (10.5 wt. %) as well as due to the addition of PEG additives and TiO_2 NPs together with the type of solvent used and type of de-mixing occurred. Therefore, the high porosity result for CA (additive free) membranes is due the instantaneous de-mixing that occurred during the phase inversion process as previously explained. On the other hand, the effect of PEG additive as pore-former and TiO_2 NPs as hydrophilicity enhancer was also accredited to the highest pore sizes and porosity results of the membranes with PEG additive and TiO_2 NPs, though a relatively delayed de-mixing was observed. One point which should be clarified here is that the delayed de-mixing, in this case, is not extended delayed de-mixing. Normally, if the delayed de-mixing is extended, the polymer film thickness will decrease considerably which may cause a decrease in the porosity of the sublayer membranes [3]. However, the CA-TiO_2 gained the lowest porosity due the NPs agglomeration phenomenon as explained previously. It can also be seen from the results that an increase in the EWC of the membrane after the addition of PEG additive is because the PEG is known for its hydrophilicity properties.

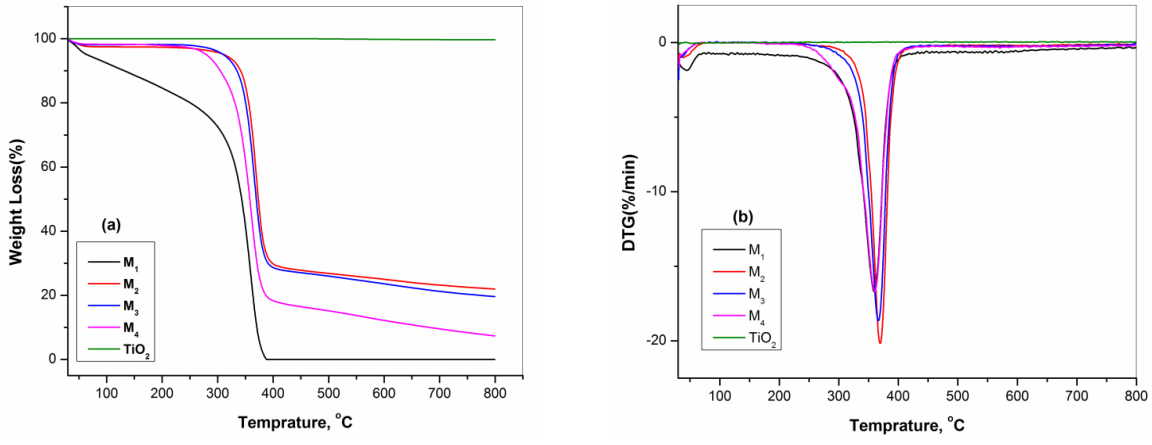

Fig. 5. (a) TGA and (b) DTG analysis results of M_1 (CA), M_2 (CA-TiO_2), M_3 (CA-PEG-TiO_2), M_4 (CA-PEG) membranes and TiO_2 NPs.

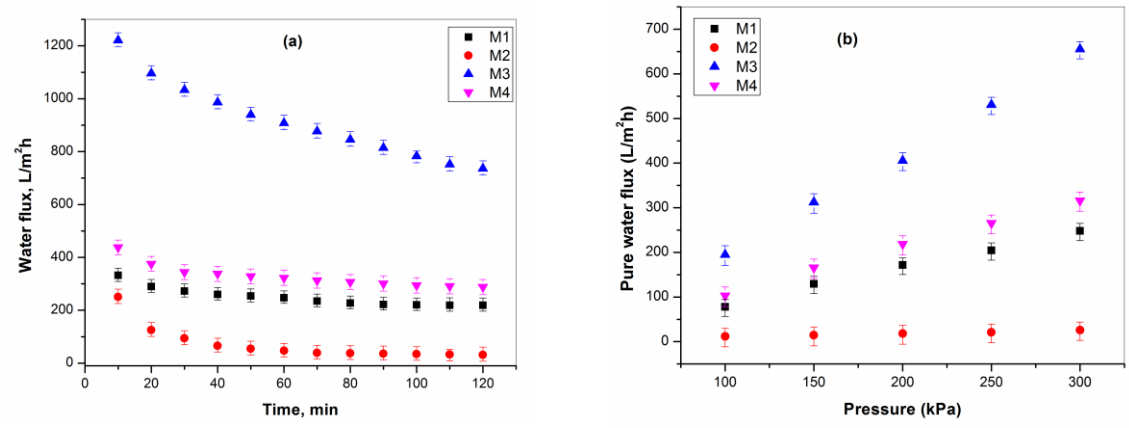

Fig. 6. (a) PWF profile during compaction study (at 300 kPa), (b) Effect of transmembrane pressure on PWF.

The influences of compaction time on the pure water flux of the prepared membranes are shown in Figure 6 (a). It is seen from the figure that the PWFs of all the membranes were observed to decrease slowly with increasing time because of the pore compaction and lastly the steady state fluxes were reached approximately after 80 min filtration operation. The gradual decrease in PWF results can be described because the compaction of pore walls attain more uniform and denser structures and cause the pore size and the flux to decrease [4]. Consequently, it is crucial to explore the effect of PEG additive on the membranes compaction process, where the effect of the PEG additive was significantly observed from this study. Another important point, which is observed during the compaction study, was that the membranes without PEG additive (i.e. M_1 and M_2) revealed lower PWFs when compared with the membranes having PEG additive (M_3 and M_4). The PWF values at 250 kPa, for M_3 and M_4 are 530.7 and 265 L/m^2 h, respectively; whereas these values are 204.5 and 21.1 L/m^2 h, respectively, for M_1 and M_2 as presented in Table 2. It is clear from the results that the introduction of hydrophilic PEG additive to the membrane casting solution helps these membranes to be porous and more hydrophilic [34]. The lowest PWF for M_2 can be explained due to the blockage of pores due to aggregation of the TiO_2 NPs inside the membrane matrix as already explained in section 3.1.1. On the other hand, the membranes with PEG additive (M_3) have shown the highest PWF result. This result obviously indicates that the introduction of PEG additive influences the membrane in two ways: (1) development of pores in the membrane structure and (2) enhancement of the hydrophilic nature of the membrane [35]. In the present study, by adding of the hydrophilic additive, the trace amount of PEG may permanently exist tangled in the membrane matrix. The presence of PEG additive can enhance the hydrophilic nature of the CA membranes. Hence, the PEG additive can play a significant role in the formation of the porous membrane with improving its hydrophilic nature, which is again directly related to its water permeability performance. Comparing both the membranes with PEG additive (i.e. M_3 and M_4), the CA-PEG-TiO_2 membrane gained higher flux than the CA-PEG membrane. These results are also confirmed by the porosity measurements reported in Table 2, where the presence of the TiO_2 NPs in the CA-PEG-TiO_2 membrane could interfere with the de-mixing process and help the formation of additional pores. On the other hand, the hydrophilic nature of TiO_2 NPs can also play an important role on increasing the flux result of the CA-PEG-TiO_2 membrane.

It is well known that the flux properties of the membrane can be influenced by several factors like membrane pore-size, cross-sectional morphology, skin-layer thickness and the hydrophilic nature of the membrane. Thus, the PWF of the prepared membranes in this study could be influenced by TiO_2 NPs. The introduction of the TiO_2 NPs can affect the membrane in two ways: (1) due to its hydrophilic nature which could improve the PWF and (2) its effect on the membrane morphological structure would also influence the permeation properties negatively or positively. Figure 6 (a) shows the PWF of all the prepared membranes with and without adding TiO_2 NPs. As TiO_2 is more hydrophilic than CA, the water has higher affinity for TiO_2 and therefore, PWF should increase in the CA-TiO_2 membrane (M_2). However, it can be seen from the figure that the pure water flux value for M_2 shows the lowest result. This is because the addition of TiO_2 NPs to the membrane forming polymer has caused pore blockage and pore failure in the membrane matrix due to the accumulation of the NPs [26]. Another important point that should be noted is that the hydrophilic nature of the CA membrane has its own effect on the PWF of the membrane without additive (M_1) so that it has shown better flux results than the CA-TiO_2 (M_2) due to the aggregation of the TiO_2 NPs on to CA matrix. On the other hand, membranes prepared from CA-PEG-TiO_2 resulted in the highest flux values. As already explained from the FESEM images, the presence of PEG additive promotes the formation of the porous structure. Thus, the TiO_2 NPs can play a significant role on the enhancement of the hydrophilicity of the membrane with less effect on the porosity of the prepared membrane. It is clear from the porosity (Table 2) data and the flux result (Figure 6) that the membranes with TiO_2 NPs (CA-PEG-TiO_2) gained higher porosity and water flux than the membranes without TiO_2 NPs (CA-PEG). Besides the enhancement of the hydrophilicity and porosity, the morphological structure of the CA membranes with TiO_2 NPs may be affected by the permeability properties. As TiO_2 NPs have a high affinity to water than the membrane-forming polymer, diffusion velocity of non-solvent (i.e. water) into the nascent membrane could be increased with TiO_2 NPs addition during the phase-inversion process. Furthermore, the AC: DMAc (solvent) diffusion velocity from the membrane to non-solvent (water) could also be increased by the addition of TiO_2 NPs. Based on this fact, the interaction between the membrane forming polymer and the solvent molecules could be weakened by the hindrance of NPs, so that the solvent molecules can be diffused simply from the polymer-matrix to the coagulation bath [36]. Consequently, the porosity and pore size of the TiO_2 entangled (i.e. CA-PEG-TiO_2) membrane were higher than those of the membranes without TiO_2 NPs (CA-PEG). The effect of PEG as a pore former as well as hydrophilicity enhancer was also accredited.

3.3.2. Membrane hydrophilicity and TiO_2 NPs stability

The hydrophilicity of the prepared membranes was studied by measuring the WCA and the drop age, defined as the duration of the water droplet on the surface of the membrane and spreading and/or permeating through the membrane cross-section [37]. The difference between WCA of all the prepared membranes is presented in Figure 7~~5~~ (a). The images of the water droplets with a volume of about 2 µL at 0.16 mL/min on the membrane surface after 60 s are shown in Figure 7~~5~~ (b). M_3 and M_4 membranes have taken about 15 s and 25 s, respectively, and show the best water wettability, where most part of the membrane surfaces were almost fully wetted and a smaller spread radius of the water drops on the top side of the membrane were detected after 60 s. On the other hand, M_1 and M_2 membranes have taken about 36 s and 32 s to initiate the surface wetting and big water drops spread radius on the top-side of the membrane was observed after 60 s (Figure 7~~5~~b). The smaller the water drop spread radius wetting area between the top and bottom surface and on the top membrane side, the better the water permeability is. As clearly observed from the graph, the WCA results of the pristine CA (M_1) membrane displays WCA at about 60±1.8º. Conversely, after the introduction of hydrophilic PEG additive and TiO_2 NPs, the M_2, M_3, and M_4 membranes displayed significantly reduced WCA results (i.e. 54.3±2.3º, 42.1±3.4º, and 45±2.0º, respectively). From these results it is clearly depicted that the contact angle results of the M_1 membrane were significantly reduced after the introduction of PEG and TiO_2 (M_2, M_3 and M_4). Membranes having smaller contact angle results are considered as more hydrophilic membranes.

The WCA results of the prepared membranes found after each soaking period are presented in Figure 7 (c)**.** The WCA values for M_1 and M_3 and M_4 have remained almost constant (i.e. 58 ±1.3 º, 42.8 ±3.3 º and 45 ±2.6 º, respectively) by increasing the soaking period in DI water. On the other hand, the WCA value of M_2 was observed to increase significantly from 51.5 ±2.2 º to 54.7 ±2.0 º, where this increase in WCA value can be accredited such that the TiO_2 NPs could leach out from matrix of the CA-TiO_2 membrane with increasing the soaking period. Conversely, no significant change in the WCA

values was observed in the case of M_3 (CA-PEG-TiO_2) with the soaking period. This interesting result is mainly accredited to the permanent existence of TiO_2 NPs within the membrane matrix and the stability of the NPs was confirmed. The stability of the NPs within the membrane matrix occurred mainly due to the introduction of PEG additive which has prevented the leaching of TiO_2 NPs, tending to an insignificant increase in WCA values during the soaking period [17].

3.4. Fouling and rejection performance study

3.4.1. Effect of PEG and TiO_2 NPs on fouling

The fouling performances of all the prepared membranes are presented in the Figure 8(a). In this study, the effect of PEG and TiO_2 were evidently detected from the fouling experiments. It is clearly observed from the figure that the PWF and BSA flux results for M_1 and M_2 are less than that of M_3 and M_4. As already explained in section 3.3, these results were attained due to the introduction of PEG and TiO_2 on the membrane matrix in M_3 and M_4 modifies the hydrophilicity and porosity of the membranes. However, the lowest flux results for M_2 were observed because of the less porosity due to the aggregation of TiO_2 on the membrane surfaces and pore channels of the membrane (section 3.1.1, morphology study). It is clear from the results that the M_1 and M_2 membranes displayed less PWF as well as the BSA fluxes due to their less hydrophilic nature and less pore formation. The improvement of pure water and BSA fluxes for M_3 and M_4 membranes were attributed to the pore-forming effect and hydrophilic nature of PEG and TiO_2, respectively [29]. However, the hydrophilic effect of TiO_2 in the case of the M_2 membrane is dominated by the pore blockage (i.e. less porous membrane). On the other hand, apart from the formation of the porous membrane, a trace amount of PEG may entangle within the membrane matrix permanently, and due to this reason, the hydrophilic nature of the prepared membrane may be enhanced [6]. As clearly shown in Figure 8(a), three BSA fouling/rinsing cycles are carried out for a total filtration time of 840 min. Each of the fouling experiments was performed with BSA solution with a concentration of 1 g L^{-1} for 2 h duration, and each of the rinsing experiments were done with deionized water for 30 min. The decrease in BSA fluxes with increasing time could be due to susceptible pore blocking of the membranes because of BSA protein deposition on the membrane surface, where the effect of concentration polarization was reduced by using high molecular weight of BSA (66 kDa) molecules and rigorous stirring (200 rpm) on the surface of the membrane. Moreover, the drop in initial fluxes are realized to be highly noticeable, and the ending fluxes are slowly dropped which are credited to the decrease in the porosity of the membrane due to an interior depostion of BSA protein which further leads to pore blocking. In the first cycle fouling/rinsing experiment, M_3 displayed the highest flux recovery (i.e. 94.1% of the initial value) with a flux value of 136.3 L m^{-2} h^{-1} at 150 kPa of trans permeable pressure, whereas water flux values of the M_1 and M_2 membranes declined to 31.2 L m^{-2} h^{-1} and 15.3 L m^{-2} h^{-1} respectively, (i.e. 28.6% and 65.7 % of the initial value, respectively). On the other hand, the flux result for M_4 was 134 L m^{-2} h^{-1} with a flux recovery of 88.9 % of the initial flux value. These results are achieved due to the hydrophilic nature of PEG and TiO_2 which can both minimize severe solute fouling of the membranes.

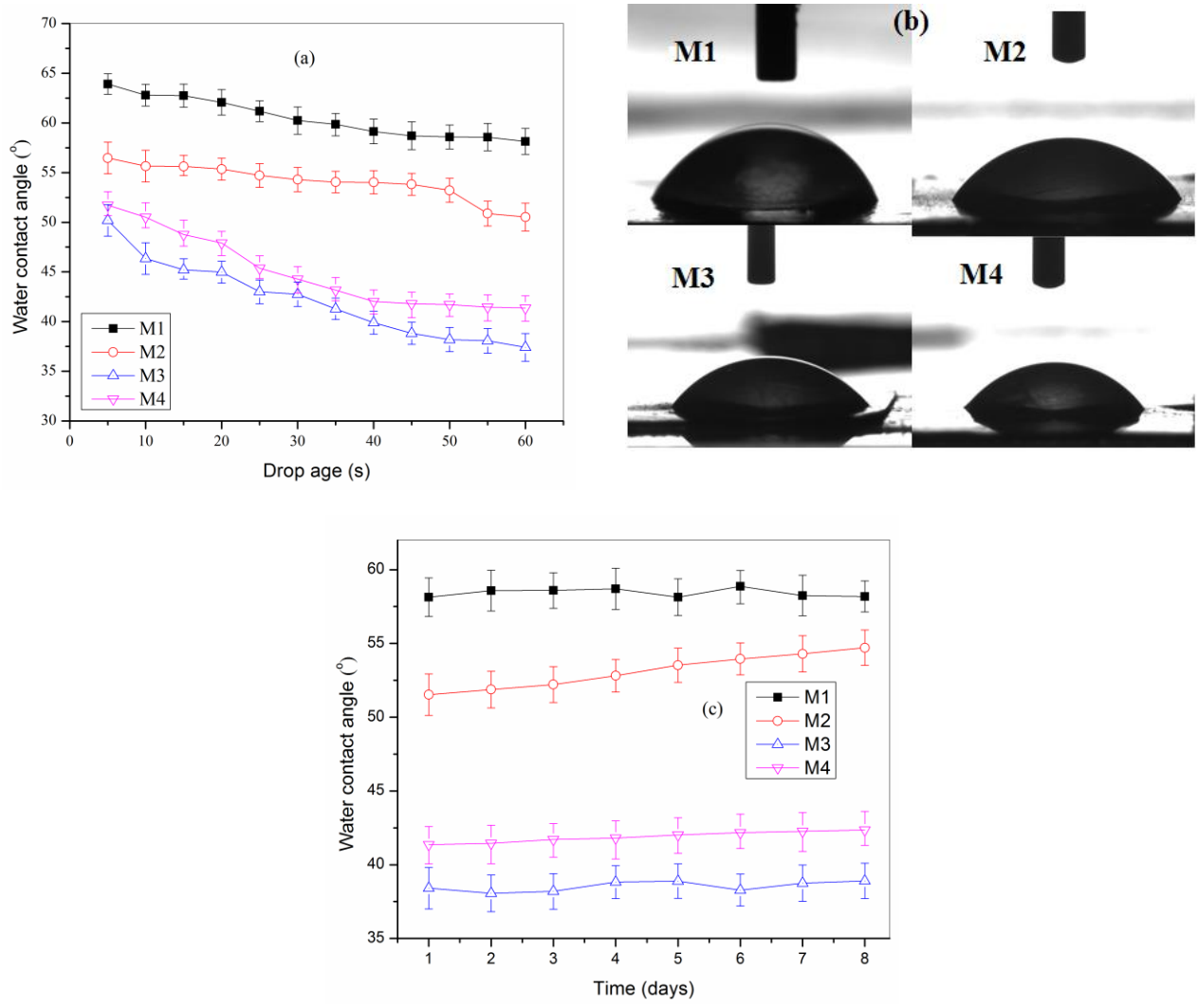

Fig. 7. (a) Water contact angle values with different drop ages; (b) images of water droplets of the prepared membranes; and (c) TiO_2 NPs stability study (Water droplet volume is about 2 µL at 0.16 mL/min).

The parameter normalized flux ratio (NFR) with filtration time (2 h) of the membranes operated for three cyles are presented in Figure 8(b). From the figure, it is clearly seen that M_3 exhibited the highest NFR values 94.1%, 88.6% and 84.1 % for cycle 1, cycle 2 and cycle 3, respectively. Moreover, these results indicate the lowest irreversible flux loss and less BSA deposition on the pore walls as well as on the surface of the membrane consistently during the three cycle operations. However, M_1 and M_2 show a significant decline in the permeate fluxes to about 28.6 % and 65.7 %, respectively, of the initial flux during the first cycle operation. Moreover, as seen from Table 3, the irreversible fouling (F_{ir}) results in the first cycle are high enough where their tendency to be fouled would be maximum. To further examine the anti-fouling properties of the prepared membranes and to study the effect of additives, the flux losses viz. total fouling (F_t), reversible fouling (F_r) and irreversible fouling (F_{ir}) were calculated, and the results are presented in Table 3. On the other hand, the increase in NFR results for M_1 and M_2 during the second and third cycle operations may be due to the development of a cake layer because of the high irreversible fouling where their flux was too low, and the flux value difference was insignificant. These results are achieved because the porosity and hydrophilicity effect could play an important role on their anti-fouling and flux properties as already explained in the pure water flux study. Moreover, the NFR results of M_4 are 88.9 %, 88.3 % and 79.1 % for the first, second, and third cycle operations, respectively. However, these results are still less than that of the M_3 membrane, where it is clear that the introduction of TiO_2 has played a crucial role in the enhancement of hydrophilicity and membrane anti-fouling property. Normally, the orders of flux recoveries for the examined membranes were consistent with their hydrophilicity and porosity nature. Therefore, the PEG free membranes are more likely prone to pore-blockage and fouling because of protein deposition than those of membranes with PEG. It is mentioned in the literature that the PEG [38] has the potential to minimize membrane fouling because of protein deposition [39]. In this study, M_3 exhibited better anti-fouling properties in the dynamic fouling process than M_1, M_2 and M_4 membranes. Therefore, the combined effect of PEG and TiO_2 could have played a significant role in a higher resistance towards membrane fouling due to BSA deposition by reducing the hydrophobic interaction between the BSA protein and membrane surface. Desorption of the deposited BSA proteins was performed by soaking the samples in water for 30 min. It was also confirmed that PEG could efficiently avoid the irreversible deposition of the protein on the surfaces. Therefore, due to the hydrophobic interaction between PEG and BSA, the proteins might be wrapped by PEG chains, forming a protective layer in addition to the anti-fouling properties of TiO_2.

Additional focus was given to the influences of filtration resistance due to concentration polarization for all membranes. Therefore, the resistances due to concentration polarization were calculated using the resistance in series model Eq**. (11)** [40]

$$R_p = \frac{\Delta P}{\mu J_{BS}} - R_m - R_f \quad (11)$$

where R_m is the membrane resistance, which is the reciprocal of the hydraulic permeability (P_m); R_f is the resistance of the fouled membrane layer which was determined after rinsing with DI water and by subtracting the resistance of the clean membrane and J_{bs} is the steady state BSA protein flux. The total fouling resistance of all the membranes was thus due to both internal membrane fouling (deposition) and the formation of a cake/gel layer on the membrane surface. The detailed results for the resistance to the BSA flux due to the membrane, fouled layer and concentration polarization for the three-filtration cycles are presented in Table 4. As clearly presented in Table 4, the results of the fouling resistance due to concentration polarization (R_P) for M_3 are low in the three cycles when compared to the other membranes (i.e. M_1, M_2, and M_4). Therefore, the effect of concentration polarization on the membrane surface was reduced due to the introduction of PEG and TiO_2 simultaneously. These results are consistent with the flux recovery results of the membrane were the highest values were attained (Table 3), and it was accredited to the best anti-fouling property of the M_3 membrane as already discussed in the previous sections.

3.4.2.Rejection performance

The BSA rejection performances of the prepared membranes are shown in Figure 9. The maximum BSA rejection values 98.4 % and 91.6% were attained for M_2 and M_1 membranes, respectively. On the other hand, the rejection results for M_3 and M_4 membranes are 88.9 % and 85.9 %, respectively. It is clearly explained in the morphology analysis section that the PEG free membranes have less porous structures, in which a better resistance to protein molecules was detected. However, the slight increase in BSA rejection for the M_3 membrane could be due to the effect of TiO_2 addition to the membrane matrix. The characteristic BSA rejection can be described using the protein deposition/repulsion phenomenon as already explained above. The prepared membranes could become more negatively charged after an introduction of TiO_2 NPs due to more negatively charged carboxylic groups along with –OH and Ti–OH groups present on the surfaces and within the matrices of the membranes [41]. Furthermore, as a pH of 7.0 is far from isoelectric point (IEP=4.9), the BSA protein becomes more negatively charged and a stronger electrostatic repulsion between BSA and the modified membranes was suggested [42]. However, some of the BSA removal characteristics can also be described using the protein deposition phenomenon onto the membrane surface in this pH range, which could be accredited to structural interaction. In addition to the electrostatic repulsion phenomena, the highest BSA removal for the M_2 and M_3 membrane was also considered as an indicator of considerable protein removal due to its structural interaction. The BSA removal phenomenon for M_1 and M_4 membranes can be suggested due to a substantial protein deposition inside and on the membrane surfaces. Therefore, the surface depositions of BSA proteins can provide an extra hindrance to solute transportation. The high rejection and comparatively lowest flux of M_2 and M_1 membranes than M_4 and M_3 can also be seen from the morphological study of their cross-section as discussed in section **3.1.** Moreover, all the experimental results were consistent with the membrane properties and agreed with each other.

The results presented in this work clearly show that a detailed performance evaluation was done for the prepared ultrafiltration M_3 membrane (i.e. CA-PEG-TiO_2) in this study as compared to the previous studies [6, 7, 43]. Therefore, the improved thermal stability and high anti-fouling properties of this membrane will help us to further investigate specific ultrafiltration applications. Thus, the authors strongly believe that this work will have a substantial contribution to the current state-of-the-art on the modification and enhancement of the properties of conventional cellulose acetate membranes. Future studies are necessary to fully investigate the performance characteristics of CA-PEG-TiO_2 membranes for different ultrafiltration applications.

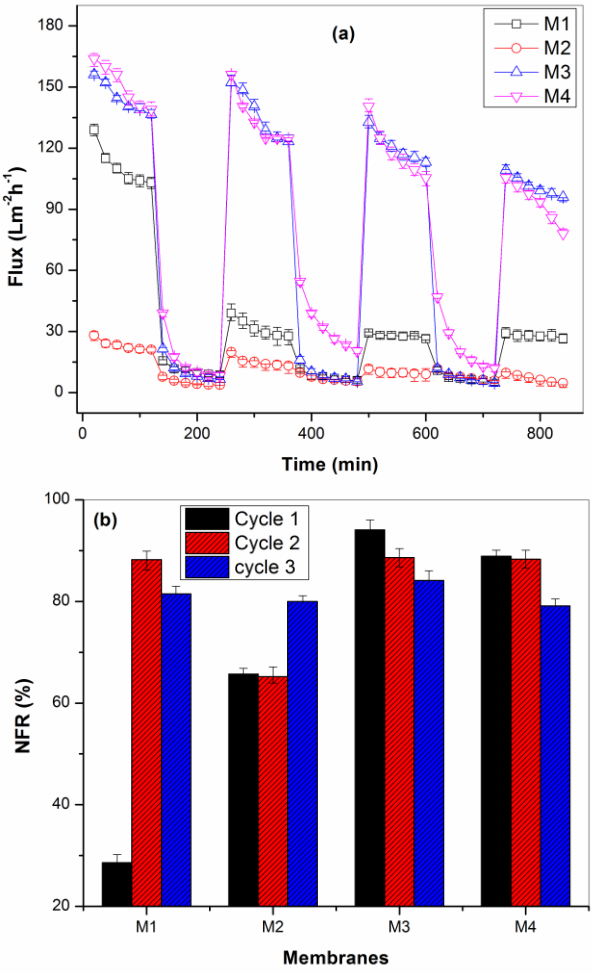

Fig. 8. (a) Permeate flux versus filtration time for M_1 (CA), M_2 (CA-TiO_2), M_3 (CA-PEG-TiO_2) and M_4 (CA-PEG) membranes: effect of PEG and TiO_2 NPs on the anti-fouling performance of the membranes (25±2 ºC, 150 kPa), (b) NFR percentage results.

Table 3
Results for flux losses caused by total fouling (F_t), reversible fouling (F_r) and irreversible fouling (F_{ir}), of the three cycles.

Membrane	First cycle				Second cycle				Third cycle			
	F_t	F_r	F_{ir}	NFR	F_t	F_r	F_{ir}	NFR	F_t	F_r	F_{ir}	NFR
M_1	0.90	0.21	0.71	28.6	0.75	0.61	0.15	85.2	0.73	0.55	0.19	81.5
M_2	0.78	0.44	0.34	65.7	0.54	0.20	0.35	65.4	0.21	0.01	0.20	80
M_3	0.92	0.87	0.06	94.1	0.93	0.82	0.11	88.6	0.94	0.78	0.16	84.1
M_4	0.89	0.78	0.11	88.9	0.77	0.64	0.12	88.3	0.81	0.60	0.21	79.1

Table 4
Results for resistances due to the membrane (R_m), fouled layer (R_f) and polarization (R_P) of the three cycles.

Membrane	First cycle				Second cycle				Third cycle			
	$\Delta p/\mu J_{bs}$	R_f	R_m	R_p	$\Delta p/\mu J_{bs}$	R_f	R_m	R_p	$\Delta p/\mu J_{bs}$	R_f	R_m	R_p
M_1	7.78	1.37	0.55	3.58	7.79	1.62	0.55	5.61	8.49	1.62	0.55	6.32
M_2	8.73	1.37	2.60	8.05	8.73	3.50	2.06	2.62	7.72	4.99	2.60	2.92
M3	1.86	0.02	0.42	3.37	1.86	0.08	0.40	1.37	2.67	0.18	0.40	2.07
M_4	6.82	0.05	0.40	5.17	6.82	0.11	0.41	6.30	13.6	0.25	0.42	12.9

** All the units are in ($\times 10^{-10}$ m^{-1})*

4. Conclusions

In the present work, the effects of PEG and TiO_2 on the preparation of the phase inverted CA ultrafiltration membrane blended with TiO_2 (i.e. CA-PEG-TiO_2) were investigated, and the following conclusions were made:

- In the case of the M_2 (CA-TiO_2) membrane, some of the TiO_2 observed to be aggregated on the surface of the membrane pores. The NPs agglomeration led to a non-uniform dispersion of the NPs within the polymer surface and structure.
- TiO_2 NPs are highly stable at high temperatures and the degradation temperature of the M_1 and M_4 were significantly improved after the addition of TiO_2. The thermal stability of M_3 exhibited higher degradation temperature than the M_1 and M_4. The slight improvement in degradation temperature for the M_2 was due to the less porous sublayer structure and strong resistance to heat flow than that of the porous membrane (M_3).
- The introduction of both PEG additive and TiO_2 NPs simultaneously plays an important role in the improvement of the thermal stability of the membrane, hydrophilicity, porosity and antifouling performance.
- Membranes without PEG additive (i.e. M_1 and M_2) revealed lower PWFs when compared with the membranes having PEG additive (M_3 and M_4). The PWF values at 250 kPa, for M_3 and M_4 are 530.7 and 265 L/m^2 h, respectively; whereas these values are 204.5 and 21.1 L/m^2 h, respectively for M_1 and M_2. The highest PWF was attained for the M_3 (CA-PEG-TiO_2).
- The maximum BSA rejection values of 98.4 % and 91.6% were attained for M_2 and M_1 membranes, respectively. The rejection results for M_3 and M_4 membranes are 88.9 % and 85.9 %, respectively. CA-TiO_2 blended with the PEG membrane (i.e. M_3) exhibited the highest BSA flux permeates and flux recovery ratios for the three fouling/rinsing cycles.

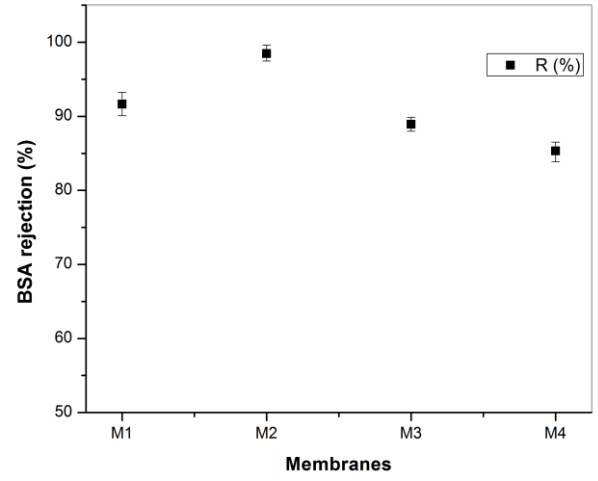

Fig. 9. BSA rejection performances of M_1 (CA), M_2 (CA-TiO_2), M_3 (CA-PEG-TiO_2) and M_4 (CA-PEG) membranes: effect of PEG and TiO_2 NPs (25±2 °C, 150 kPa).

5. Acknowledgements

Central Instruments Facility (CIF), IIT Guwahati, India is gratefully acknowledged by the authors for allowing us to use FESEM and Prof. Bishnupada Mandal, Department of Chemical Engineering, IIT Guwahati for providing us his casting knife.

6. References

[1] M.-L. Luo, J.-Q. Zhao, W. Tang, C.-S. Pu, Hydrophilic modification of poly(ether sulfone) ultrafiltration membrane surface by self-assembly of TiO_2 nanoparticles, App. Surf. Sci. 249 (2005) 76-84.
[2] S. Zhao, Z. Wang, X. Wei, X. Tian, J. Wang, S. Yang, S. Wang, Comparison study of the effect of PVP and PANI nanofibers additives on membrane formation mechanism, structure and performance, J. Membr. Sci. 385-386 (2011) 110-122.
[3] B. Reuvers, Membrane formation mechanism: diffusion indused de-mixing processes in ternary polymeric system, PhD thesis, University of Twente, 1987.
[4] M. Mulder, Basic Principles of Membrane Technology, 1st ed., Kluwer academic Publishers, Dordrecht, The Netherlands, 1996.
[5] M. Algarra, M.I. Vázquez, B. Alonso, C.M. Casado, J. Casado, J. Benavente, Characterization of an engineered cellulose based membrane by thiol dendrimer for heavy metals removal, Chem. Eng. J. 253 (2014) 472-477.
[6] G. Arthanareeswaran, P. Thanikaivelan, K. Srinivasn, D. Mohan, M. Rajendran, Synthesis, characterization and thermal studies on cellulose acetate membranes with additive, Eur. Polym. J. 40 (2004) 2153-2159.
[7] E. Saljoughi, M. Amirilargani, T. Mohammadi, Effect of PEG additive and coagulation bath temperature on the morphology, permeability and thermal/chemical stability of asymmetric CA membranes, Desalination 262 (2010) 72-78.
[8] Y. Liu, G.H. Koops, H. Strathmann, Characterization of morphology controlled polyethersulfone hollow fiber membranes by the addition of polyethylene glycol to the dope and bore liquid solution, J. Membr. Sci. 223 (2003) 187-199.
[9] S.R. Panda, S. De, Role of polyethylene glycol with different solvents for tailor-made polysulfone membranes, J. Polym. Res. 20 (2013) 179.
[10] B. Chakrabarty, A.K. Ghoshal, M.K. Purkait, Effect of molecular weight of PEG on membrane morphology and transport properties, J. Membr. Sci. 309 (2008) 209-221.
[11] F. Shi, Y. Ma, J. Ma, P. Wang, W. Sun, Preparation and characterization of PVDF/TiO_2 hybrid membranes with different dosage of nano-TiO_2, J. Membr. Sci. 389 (2012) 522-531.
[12] X. Cao, J. Ma, X. Shi, Z. Ren, Effect of TiO2 nanoparticle size on the performance of PVDF membrane, App. Surf. Sci. 253 (2006) 2003-2010.
[13] N. Maximous, G. Nakhla, W. Wan, K. Wong, Preparation, characterization and performance of Al_2O_3/PES membrane for wastewater filtration, J. Membr. Sci. 341 (2009) 67-75.
[14] A. Bottino, G. Capannelli, A. Comité, Preparation and characterization of novel porous PVDF-ZrO_2 composite membranes, Desalination 146 (2002) 35-40.
[15] J. Lin, W. Ye, K. Zhong, J. Shen, N. Jullok, A. Sotto, B. Van der Bruggen, Enhancement of polyethersulfone (PES) membrane doped by monodisperse Stöber silica for water treatment, Chem. Eng. Proc.: Proc. Intens. 107 (2016) 194-205.
[16] J.A. Prince, S. Bhuvana, K.V.K. Boodhoo, V. Anbharasi, G. Singh, Synthesis and

characterization of PEG-Ag immobilized PES hollow fiber ultrafiltration membranes with long lasting antifouling properties, J. Membr. Sci. 454 (2014) 538-548.
[17] J. Garcia-Ivars, M.-I. Iborra-Clar, M.-I. Alcaina-Miranda, J.-A. Mendoza-Roca, L. Pastor-Alcañiz, Development of fouling-resistant polyethersulfone ultrafiltration membranes via surface UV photografting with polyethylene glycol/aluminum oxide nanoparticles, Sep. Purif. Technol. 135 (2014) 88-99.
[18] C.S. Ong, W.J. Lau, P.S. Goh, B.C. Ng, A.F. Ismail, Preparation and characterization of PVDF–PVP–TiO_2 composite hollow fiber membranes for oily wastewater treatment using submerged membrane system, Desal. Wat. Treat. (2013) 1-11.
[19] E. Yuliwati, A.F. Ismail, Effect of additives concentration on the surface properties and performance of PVDF ultrafiltration membranes for refinery produced wastewater treatment, Desalination 273 (2011) 226-234.
[20] G. Wu, S. Gan, L. Cui, Y. Xu, Preparation and characterization of PES/TiO_2 composite membranes, Appl. Surf. Sci. 254 (2008) 7080-7086.
[21] Y. Zhao, L. Zhu, Z. Yi, B. Zhu, Y. Xu, Improving the hydrophilicity and fouling-resistance of polysulfone ultrafiltration membranes via surface zwitterionicalization mediated by polysulfone-based triblock copolymera dditive, J. Membr. Sci. 440 (2013) 40–47.
[22] R. Guan, H. Dai, C. Li, J. Liu, J. Xu, Effect of casting solvent on the morphology and performance of sulfonated polyethersulfone membranes, J. Membr. Sci. 277 (2006) 148–156.
[23] J. Qin, Y. Li, L. Lee, H. Lee, Cellulose acetate hollow fiber ultrafiltration membranes made from CA/PVP 360 K/NMP/water, J. Membr. Sci. 218 (2003) 173–183.
[24] R. Boom, I. Wlenk, T. Boomgaard, C. Smolders, Microstructures in phase inversion membranes. Part 2. The role of a polymeric additive, J. Membr. Sci. 73 (1992) 277-292.
[25] C. Smolders, A. Reuvers, R. Boom, I. Wienk, Microstructures in phase-inversion membranes. Part 1. Formation of macrovoids, J. Membr. Sci. 73 (1992) 259-275.
[26] J. Garcia-Ivars, M.-I. Iborra-Clar, M.-I. Alcaina-Miranda, B. Van der Bruggen, Comparison between hydrophilic and hydrophobic metal nanoparticles on the phase separation phenomena during formation of asymmetric polyethersulphone membranes, J. Membr. Sci. 493 (2015) 709-722.
[27] L.F. Greenlee, N.S. Rentz, Influence of nanoparticle processing and additives on PES casting solution viscosity and cast membrane characteristics, Polymer 103 (2016) 498-508.
[28] A. Sotto, A. Boromand, R. Zhang, P. Luis, J.M. Arsuaga, J. Kim, B. Van der Bruggen, Effect of nanoparticle aggregation at low concentrations of TiO_2 on the hydrophilicity, morphology, and fouling resistance of PES–TiO_2 membranes, J. Coll. Interf. Sci. 363 (2011) 540-550.
[29] K.H. Chan, E.T. Wong, M. Irfan, A. Idris, N.M. Yusof, Enhanced Cu(II) rejection and fouling reduction through fabrication of PEG-PES nanocomposite ultrafiltration membrane with PEG-coated cobalt doped iron oxide nanoparticle, J. Taiwan. Inst. Chem. Eng. 47 (2015) 50-58.
[30] M. Zafar, M. Ali, S.M. Khan, T. Jamil, M.T.Z. Butt, Effect of additives on the properties and performance of cellulose acetate derivative membranes in the separation of isopropanol/water mixtures, Desalination 285 (2012) 359-365.
[31] M.d.C.C. Lucena, A.E. V. de Alencar, S.E. Mazzeto, S.d.A. Soares, The effect of additives on the thermal degradation of cellulose acetate, Polym. Degrad. Stab. 80 (2003) 149-155.
[32] M. Ali, M. Zafar, T. Jamil, M.T.Z. Butt, Influence of glycol additives on the structure and performance of cellulose acetate/zinc oxide blend membranes, Desalination 270 (2011) 98-104.
[33] P.S.T. Machado, A.C. Habert, C.P. Borges, Membrane formation mechanism based on precipitation kinetics and membrane morphology: flatat and hollow fiber polysulfone membranes, J. Membr. Sci. 155 (1999) 171-183.
[34] J. Marchese, M. Ponce, N. Ochoa, P. Prádanos, L. Palacio, A. Hernández, Fouling behaviour of polyethersulfone UF membranes made with different PVP, J. Membr. Sci. 211 (2003)1–11.
[35] D.B. Mosqueda-Jimenez, R.M. Narbaitz, T. Matsuura, G. Chowdhury, G. Pleizier, J.P. Santerre, Influence of processing conditions on the properties of ultrafiltration membranes, J. Membr. Sci. 231 (2004) 209-224.
[36] T.-H. Bae, T.-M. Tak, Effect of TiO_2 nanoparticles on fouling mitigation of ultrafiltration membranes for activated sludge filtration, J. Membr. Sci. 249 (2005) 1-8.
[37] H. Shi, Y. He, Y. Pan, H. Di, G. Zeng, L. Zhang, C. Zhang, A modified mussel-inspired method to fabricate TiO_2 decorated superhydrophilic PVDF membrane for oil/water separation, J. Membr. Sci. 506 (2016) 60-70.
[38] S. Robinson, P. Williams, Inhibition of Protein Adsorption onto Silica by Polyvinylpyrrolidone, Langmuir 18 (2002) 8743-8748.
[39] J. Wu, Z. Wang, W. Lin, S. Chen, Investigation of the interaction between poly(ethylene glycol) and protein molecules using low field nuclear magnetic resonance, Act. Biomater. 9 (2013) 6414-6420.
[40] B. Kwon, J. Molek, A. Zydney, Ultrafiltration of PEGylated proteins: Fouling and concentration polarization effects, J. Membr. Sci. 319 (2008) 206-213.
[41] M. Kumar, Z. Gholamvand, A. Morrissey, K. Nolan, M. Ulbricht, J. Lawler, Preparation and characterization of low fouling novel hybrid ultrafiltration membranes based on the blends of GO−TiO_2 nanocomposite and polysulfone for humic acid removal, J. Membr. Sci. 506 (2016) 38-49.
[42] H. Mo, K.G. Tay, H.Y. Ng, Fouling of reverse osmosis membrane by protein (BSA): Effects of pH, calcium, magnesium, ionic strength and temperature, J. Membr. Sci. 315 (2008) 28-35.
[43] R. Abedini, S.M. Mousavi, R. Aminzadeh, A novel cellulose acetate (CA) membrane using TiO_2 nanoparticles: Preparation, characterization and permeation study, Desalination 277 (2011) 40-45.